Pulsing to Improve Bubble Column Performance: II. Jetting Gas Rates

F. Carl Knopf, Yogesh Waghmare, Jia Ma, and Richard G. Rice
Dept. of Chemical Engineering, Louisiana State University, Baton Rouge, LA 70803

DOI 10.1002/aic.10699
Published online November 1, 2005 in Wiley InterScience (www.interscience.wiley.com).

The bubble column reactor (BCR) used in Part I was subjected to forced oscillations at high gas rates under jetting conditions. Two piston types were used: a flexible rubber membrane as used in Part I and a modification thereof to cause a more rigid, stiff piston behavior. The mass transfer performance differences between the piston types were quite remarkable, the former yielding peaking with respect to increased frequency and the latter produced monotonic increases up to an asymptote as the frequency was increased. The Benjamin–Ursell stability theory was found useful in tracking regimes of maximum enhancement. © 2005 American Institute of Chemical Engineers *AIChE J,* 52: 1116–1126, 2006
Keywords: oscillation, bubble columns, mass transfer

Introduction

The idea of applying pulsation to bubble columns for the purpose of mass transfer enhancement is quite old, notwithstanding recent efforts.[1-4] Early experiments by Bretsznajder et al.[5] and Harbaum and Houghton[6] showed substantial improvements in mass transfer. This effect was attributed to increased bubble hold-up, arising from induced Bjerknes "kinetic buoyancy" according to Baird.[7] Baird[8] also provided corrections to the well-known bubble natural frequency originally derived by Minnaert,[9] who found that

$$\omega_n = \frac{1}{r_0}\left(\frac{3\gamma P_0}{\rho_l}\right)^{1/2} \tag{1}$$

and the Baird correction for finite columns yielded

$$\omega_n = \frac{1}{r_0}\left(\frac{3\gamma P_0}{\rho_l}\right)^{1/2}\left[1 + \left(\frac{r_0}{R}\right)\left(\frac{4L}{R} - 1\right)\right]^{-1/2} \tag{2}$$

It was previously thought that forced oscillations must match the Minnaert natural frequency to cause unstable bubble breakup. For a 3 mm diameter spherical bubble at near atmospheric pressure, this would require pulsing at approximately 2200 Hz. However, significant improvements have been reported in the range 10–150 Hz, with peaking at certain frequencies.[10] The halting or retardation of rising bubbles has been explained[11] by the Bjerknes force acting downward. According to this simple theory a bubble is halted by vibrations if M is unity, where

$$M = \frac{\omega^4 A^2 \rho_l h}{2gP_0} \tag{3}$$

Most industrial operations operate at high gas rates, such that jetting occurs at the gas injection port. The following expression in Wallis[12] shows that jetting occurs when the gas velocity from the orifice is such that

$$\frac{V_g\sqrt{\rho_g}}{[g\sigma(\rho_l - \rho_g)]^{1/4}} > 1.25\left[\frac{\sigma}{g(\rho_l - \rho_g)R_0^2}\right]^{1/2} \tag{4}$$

For air in water, an 0.75 mm ID injector will jet when gas flow exceeds 14 mL/s.

Under jetting conditions, large gas slugs form with a wide distribution in sizes. Figure 1a shows the bubbles created downstream from a single stainless steel injector (ID = 0.75 mm) that is operating at jet flow conditions. Some large,

Correspondence concerning this article should be addressed to F. C. Knopf at knopf@lsu.edu or R. G. Rice at dickrice@wwgap.net.

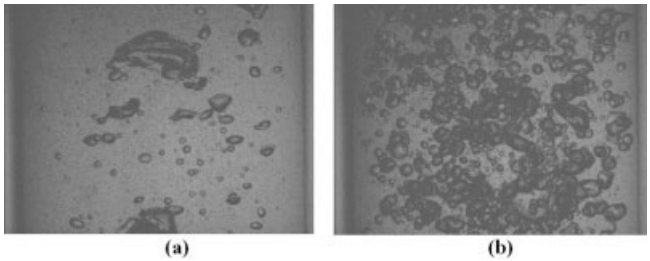

Figure 1. Photograph of bubble column showing gas dispersion.

Photograph is taken at 350 mm above nozzle. Q_g = 36.4 mL/s (superficial nozzle gas velocity = 46.3 m/s): (a) no forcing; (b) with forcing, f = 16 Hz, cam amplitude = 1.36 mm.

unstable bubbles are formed in the column proper, but there is also a wide distribution of bubble sizes because there is some bubble breakup at the injector tip. This is typical of unforced steady-state injection at high gas feeds and results from gas jet instability controlled by surface tension and shear. Many of the slugs rise as spherical-cap bubbles with nearly flat undersides. We observed reductions in bubble size when such jetted columns were subjected to pulsing in the range 10–30 Hz as shown in Figure 1b. We sought to determine whether intensification could improve performance under such maldistribution of bubbles.

Experimental

The experimental equipment consists of a bubble column with a single air injector.[13] The details of the experimental rig are described in Part I. Special note must be given to the novel piston design, which is now modified in Part II of this study.

Amplitude measurements

The natural gum rubber sheet at the base of the column is clamped between two stainless steel disks. For the high flow experiments, different disk sizes were used. To create a *flexible piston*, each disk was 2.73 cm in diameter. The column diameter is 8.9 cm, which effectively allows pulsation of 56.3 cm^2 of rubber at the column base. Data for true fluid amplitude (A^*) as a function of cam setting, oscillation frequency, and membrane thickness are given in Tables 1 and 2 of Part I.

To create a more *rigid piston*, the natural gum rubber sheet at the base of the column is clamped between two stainless steel disks each 8.26 cm in diameter. This allows pulsation of only 2.74 cm^2 of rubber at the column base, which will behave more like a solid piston. Here the fluid amplitude (A) was experimentally verified to be the cam setting.

Voidage (gas hold-up) measurements

The gas hold-up was determined by the manometric method.[14] Two taps are used, one 11 cm from the rubber sheet and the other 77 cm above the rubber sheet. The manometer fluid is Meriam Red 295, with a specific gravity of 2.95. A pressure balance on each leg of the manometer allows voidage (ε) to be determined using

$$\varepsilon = \left(\frac{\rho_m - \rho_l}{\rho_l}\right)\frac{\Delta h}{H} \tag{5}$$

The height differential in Meriam Red 295 (Δh) was determined using a cathetometer that provided an accuracy of ± 0.01 mm. Here H is the distance between the two taps.

Mass-transfer measurements

A key aspect of the forcing technology is to improve mass transfer. The generation of large bubble numbers, and consequently large surface area, using low energy input may allow agitator replacement with savings. To investigate improvements in mass transfer, we measured the mass transfer coefficient (k_La) as a function of frequency at several air flow rates and amplitudes. The same equipment and equations as Part I were again used, and for initially clean solutions ($C_0 = 0$), the solution as before is

$$\frac{C(t)}{C^*} = 1 - \exp(-k_L a t) \tag{6}$$

The only unknown here is k_La, which is determined by minimizing the sum of the square of the difference between measured and predicted normalized concentration measurements. The standard regression solver in Excel was used. Concentration measurements were collected every 0.33 s and then every 10 data points were averaged and stored.

Results and Discussion

We tested the two types of pistons mentioned earlier: a flexible piston and a more rigid design. The former sustains considerable dynamics attributed to elasticity, whereas the latter acts more like a solid piston.

Mass transfer and voidage measurements: flexible piston

In this part, gas pressure—and thus gas flow—is sufficiently high to mitigate the suck-back phenomenon seen in Part I. For example, at a cam amplitude of 1.36 mm, suck-back occurred at a nozzle gas velocities of about 30 m/s. Above these velocities, jet flow is observed at the injector with little or no flow reversal in the injector tube. Also, for the flexible piston, dynamics arise as discussed in Part I and there is a system resonance in fluid amplitude.

At high gas flow rate and under appropriate forcing conditions, dramatic bubble breakage can be obtained as shown in Figure 1b. The jetting mode at the injector is manifested by the production of large bubbles in the immediate vicinity of the injector. However, downstream of the injector (as shown in Figure 1b) the bubbles are considerably smaller and more uniform with a tight size distribution, indicating that the large bubbles were broken. The large bubbles start to break up within approximately two column diameters of the injector and at low frequencies (of order 10 Hz).

Experiments were performed to measure the effect of vibration frequency, vibration amplitude, and gas flow rate on both the volumetric mass transfer coefficient and the gas hold-up. For these experiments, a single stainless steel injector (ID = 0.75 mm; OD = 1.5 mm; vertical length = 38 mm) was used. Tables 1 and 2 and Figures 2 and 3 summarize results for a high gas flow rate of 30.4 mL/s (superficial nozzle gas velocity of 68.8 m/s). Cam amplitudes of both 1.36 mm (Table 1) and 0.51

Table 1. Flexible Piston Results[†]

(a) Membrane thickness = 1.59 mm

At 0 Hz, A_0 = 0.74 mm and ε = 0.0113						At 0 Hz, k_La = 0.004 s^{-1}		
F (Hz)	A^* (mm)	A^*/A_0	ε^*	$\varepsilon^*/\varepsilon$	Sloshing	F (Hz)	k_La^* (s^{-1})	k_La^*/k_La
10	0.52	0.70	0.0122	1.08	No	**15**	**0.012**	**3**
15	**1.69**	**2.28**	**0.0223**	**1.97**	Yes	17.5	0.0085	2.125
17.5	1.66	2.24	0.0141	1.24	Yes			
20	0.97	1.31	0.0115	1.02	No			
22.5	0.78	1.05	0.0114	1.00	No			
25	0.71	0.96	0.0113	1.00	No			
30	0.39	0.53	0.0112	0.99	No			

(b) Membrane thickness = 3.18 mm

At 0 Hz, A_0 = 0.74 mm and ε = 0.0113						At 0 Hz, k_La = 0.004 s^{-1}		
F (Hz)	A^* (mm)	A^*/A_0	ε^*	$\varepsilon^*/\varepsilon$	Sloshing	F (Hz)	k_La^*	k_La^*/k_La
10	0.65	0.88	0.0115	1.02	No	10	0.004	1
15	1.30	1.76	0.0121	1.07	Yes	15	0.0067	1.675
17.5	**2.46**	**3.32**	**0.0208**	**1.84**	Yes	**17.5**	**0.013**	**3.25**
20	1.69	2.28	0.0135	1.20	Yes	20	0.01	2.5
22.5	1.17	1.58	0.0114	1.01	Yes	22.5	0.008	2
25	1.04	1.41	0.0107	0.95	No	25	0.006	1.5
30	0.32	0.43	0.0106	0.94	No			

(c) Membrane thickness = 6.35 mm

At 0 Hz, A_0 = 0.74 mm and ε = 0.0113						At 0 Hz, k_La = 0.004 s^{-1}		
F (Hz)	A^* (mm)	A^*/A_0	ε^*	$\varepsilon^*/\varepsilon$	Sloshing	F (Hz)	k_La^*	k_La^*/k_La
10	0.78	1.05	0.0116	1.01	No	17.5	0.012	3
15	0.84	1.14	0.0140	1.22	No	20	**0.0132**	**3.3**
17.5	1.23	1.66	**0.0260**	**2.27**	Yes	**22.5**	0.0125	3.125
20	1.69	2.28	0.0233	2.04	Yes			
22.5	**1.94**	**2.62**	0.0159	1.39	Yes			
25	1.81	2.45	0.0131	1.14	Yes			
30	1.1	1.49	0.0108	0.94	No			

[†] Cam amplitude = 1.36 mm; Q_g = 30.4 mL/s; superficial nozzle gas velocity = 68.8 m/s.

mm (Table 2) were tested with rubber sheets of three different thicknesses: 1.59 mm (1/16-in.); 3.18 mm (1/8-in.); 6.35 mm (1/4-in.). We again use an asterisk to denote the vibrated case.

We have used the notation that A^* is the fluid amplitude as a function of frequency, whereas A_0 is the fluid amplitude as frequency tends to zero. In Tables 1 and 2 we have marked (in bold) the frequency for maximum amplitude enhancement (A^*/A_0), for each of the three membranes tested. Also noted, in bold, are the maximum in mass transfer enhancement (k_La^*/k_La) and voidage enhancement ($\varepsilon^*/\varepsilon$), for each membrane. The observed maximum values in k_La^* and ε^* for the flexible piston are in general agreement with the observed maximum values in amplitude. For example, Figure 2 plots the data from Table 1b as (A^*/A_0), and the new data for jetting conditions for (k_La^*/k_La) and ($\varepsilon^*/\varepsilon$) vs. frequency all show a symmetric maximum at 17.5 Hz. Figure 2 shows maximum mass transfer enhancement of about 225%, whereas Figure 3 (data from Table 2b), with a lower cam amplitude setting, shows smaller mass transfer enhancements. At both cam settings, voidage enhancements are generally not as large as those observed for mass transfer. Referring to the dynamics of the piston system shown in Table 3 of Part I, we see at these amplitudes the natural frequencies were estimated to be 17.99 Hz for the cam amplitude of 1.36 mm and 20.37 Hz for the cam amplitude of 0.51 mm.

In Tables 1 and 2 we have also indicated whether sloshing at the top interface was observed. As will be discussed in a later section, sloshing indicates an unstable region of BCR operation. This surface instability may be linked to the observed increase in performance.

To help clarify these findings we examined the effect of gas rate using the 3.18 mm (1/8-in.) rubber sheet at the two cam settings of 1.36 and 0.51 mm. The nozzle gas velocities used were 33.9, 45.3, 56.6, and 68.8 m/s (or 15, 20, 25, and 30.4 mL/s gas flow rates). For all tested flow rates, the k_La^* values go through a steep symmetric maximum at about 17.5 Hz at the two cam settings. This maximum appears independent of nozzle gas velocities at the tested cam amplitude settings (Figures 4 and 5). At 17.5 Hz, mass transfer enhancements exceeding 200% were found for all tested flow rates at the higher cam setting (Figure 4b) and mass transfer enhancements exceeding 100% were found for tested flow rates at the lower cam setting (Figure 5b). Voidage measurements vs. frequency at two different flow rates and two cam settings (Figures 6 and 7) show a maximum at 17.5 Hz, although the voidage enhancements are again not as large as those observed for mass transfer.

The trends shown in Figures 2 to 7 lead to speculation that the flexible piston–enhanced mass transfer results may correlate with voidage or amplitude. In Figure 8 both (k_La^*/k_La)/(A^*/A_0) vs. frequency and (k_La^*/k_La)/($\varepsilon^*/\varepsilon$) vs. frequency are plotted. The fact that (k_La^*/k_La)/(A^*/A_0) $\approx$ 1 (vs. frequency) provides strong evidence that bubble breakup and enhanced mass transfer are amplitude driven when using the flexible piston at high gas velocities.

Table 2. Flexible Piston Results[†]

(a) Membrane thickness = 1.59 mm

At 0 Hz, A_0 = 0.303 mm and ε = 0.0109						At 0 Hz, k_La = 0.004 s^{-1}		
F (Hz)	A^* (mm)	A^*/A_0	ε^*	$\varepsilon^*/\varepsilon$	Sloshing	F (Hz)	k_La^*	k_La^*/k_La
10	0.38	1.25	0.0112	1.03	No	17.5	0.005	1.25
15	0.92	3.04	0.0125	1.15	No			
17.5	**1.15**	**3.80**	**0.0131**	**1.20**	Yes			
20	0.61	2.01	0.0125	1.15	No			
22.5	0.38	1.25	0.0109	1.01	No			
25	0.31	1.02	0.0111	1.02	No			
30	0.39	0.53	0.0112	0.99	No			

(b) Membrane thickness = 3.18 mm

At 0 Hz, A_0 = 0.303 mm and ε = 0.0106						At 0 Hz, k_La = 0.004 s^{-1}		
F (Hz)	A^* (mm)	A^*/A_0	ε^*	$\varepsilon^*/\varepsilon$	Sloshing	F (Hz)	k_La^*	k_La^*/k_La
15	0.52	1.72	0.0110	1.04	No	15	0.0054	1.35
17.5	0.84	2.77	**0.0140**	**1.32**	Yes	17.5	**0.0095**	**2.375**
20	**1.56**	**5.15**	0.0107	1.01	Yes	**20**	0.0056	1.4
22.5	0.91	3.00	0.0094	0.89	No	25	0.0048	1.2
25	0.39	1.29	0.0093	0.88	No			
30	0.13	0.43	0.0089	0.84	No			

(c) Membrane thickness = 6.35 mm

At 0 Hz, A_0 = 0.303 mm and ε = 0.0113						At 0 Hz, k_La = 0.004 s^{-1}		
F (Hz)	A^*	A^*/A_0	ε^*	$\varepsilon^*/\varepsilon$	Sloshing	F (Hz)	k_La^*	k_La^*/k_La
10	0.38	1.25	0.0122	1.08	No	17.5	0.005	1.25
15	0.31	1.02	0.0135	1.19	No	20	0.008	2
17.5	0.46	1.52	0.0140	1.24	No	22.5	0.008	2
20	0.61	2.01	**0.0153**	**1.35**	Yes			
22.5	0.92	3.04	0.0119	1.05	Yes			
25	**1.37**	**4.52**	0.0115	1.02	Yes			
30	0.46	1.52	0.0112	0.99	No			

[†] Cam amplitude = 0.51 mm; Q_g = 30.4 mL/s.

The evidence seems to show that the enhancement at the natural frequency of the membrane–water system arises from the increase in the liquid amplitude under conditions of resonance for this second-order system. Also, Figures 4b, 5b, 6b, and 7b suggest that the gas rate is not an important factor when results are normalized with respect to nonvibrating conditions. This suggests k_La^* for pulsing has the same gas velocity dependency as that of the steady case, k_La.

Mass transfer and voidage measurements: solid piston

The extensive dynamics caused by the elastic piston produced unique effects. It became apparent that the elasticity of

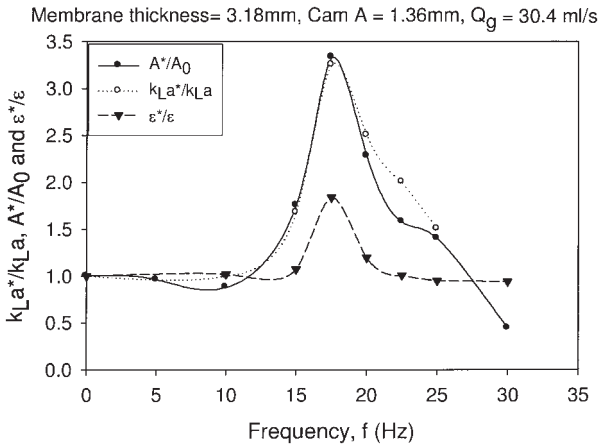

Figure 2. k_La^*/k_La, A^*/A_0, and $\varepsilon^*/\varepsilon$ as a function of frequency.

Cam amplitude = 1.36 mm, Q_g = 30.4 mL/s (superficial nozzle gas velocity = 68.8 m/s), membrane thickness = 3.18 mm.

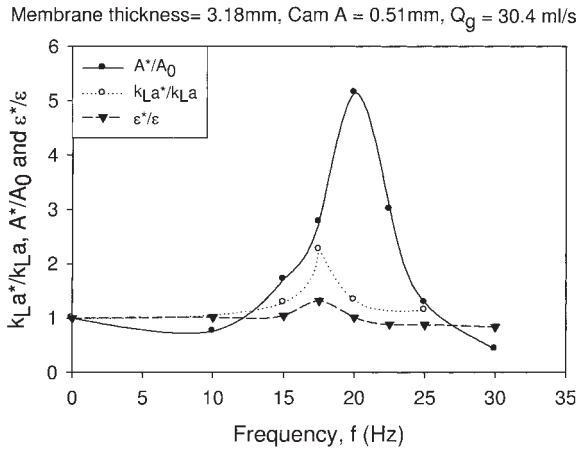

Figure 3. k_La^*/k_La, A^*/A_0, and $\varepsilon^*/\varepsilon$ as a function of frequency.

Cam amplitude = 0.51 mm, Q_g = 30.4 mL/s, membrane thickness = 3.18 mm.

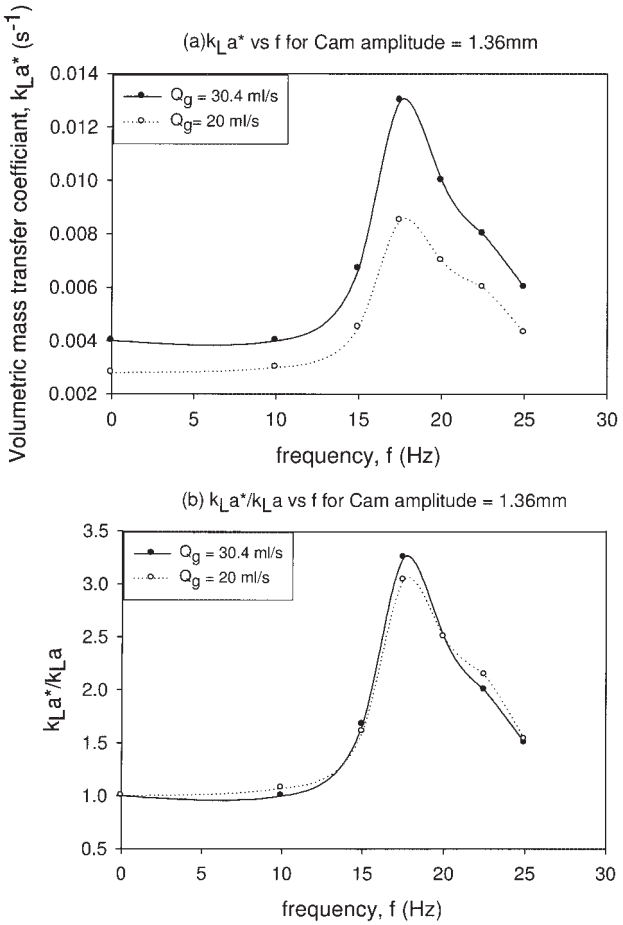

Figure 4. Volumetric mass-transfer coefficient as a function of frequency.

Cam amplitude = 1.36 mm, membrane thickness= 3.18 mm: (a) absolute k_La^*; (b) enhancement (k_La^*/k_La).

the membrane piston produced resonant behavior at certain frequencies. We wondered whether pure oscillations, using a more rigid piston, would produce different results. To create a solid piston, the natural gum rubber sheet (3.18 mm) at the base of the column is clamped between two larger stainless steel disks each 8.26 cm in diameter. The column diameter is 8.9 cm, which allows a maximum exposure of 2.74 cm^2 of rubber at the column base. This combination produces a nearly solid piston behavior so that the cam amplitude setting is the same as the fluid amplitude (A). The mass transfer enhancements for different fixed amplitudes of the solid piston at the maximum flow rate of 30.4 mL/s are given in Table 3 and plotted in Figure 9.

The solid piston produced quite different results, relative to the flexible piston. Enhancements in mass transfer in excess of 500% were observed using 2.46 mm amplitude and frequencies as low as 17.5 Hz. Enhancements in excess of 400% are possible with amplitudes as low as 1.23 mm and frequencies as low as 20 Hz. This improvement exceeds any seen so far in the literature. Sigmoidal behavior, because k_La^* was plotted vs. frequency, was observed reaching clearly defined asymptotes.

Figure 9 for the solid piston and Figure 8a for the flexible piston can be compared directly. For the solid piston no elastic resonance occurred, and thus $A/A_0 = 1$ for all frequencies. There is little agreement between these figures, especially as the amplitude and frequency are increased. We suspect that the method of pulsing—flexible vs. solid piston—may produce different flow patterns in the column, especially at higher frequencies and amplitudes.

It is possible to make some general comments about the behavior manifest in Figure 9. At constant amplitude, as the frequency increases, bubble breakage increases. This will usually occur with second-order kinetics, meaning two bubbles form from one large one. More breakage occurs as the frequency increases until a critical bubble size occurs. Beyond this point, bubbles no longer break and they retain this maximum stable size. The new surfaces created during breakage cause substantial increases in k_La^* and after the critical bubble size is reached, no further increase is possible. This possibly explains the mass transfer coefficient values reaching a plateau. This plateau phenomenon was not observed with the flexible piston because of the dynamic phase shift effects caused by the rubber membrane; the fluid amplitude reached a maximum and quickly dropped off.

We also observed column foaming and sloshing at some conditions (Table 3). Here with the solid piston at high amplitudes and frequencies, smaller bubbles are moved so violently that the surfaces are cleansed (removing surfactant film), al-

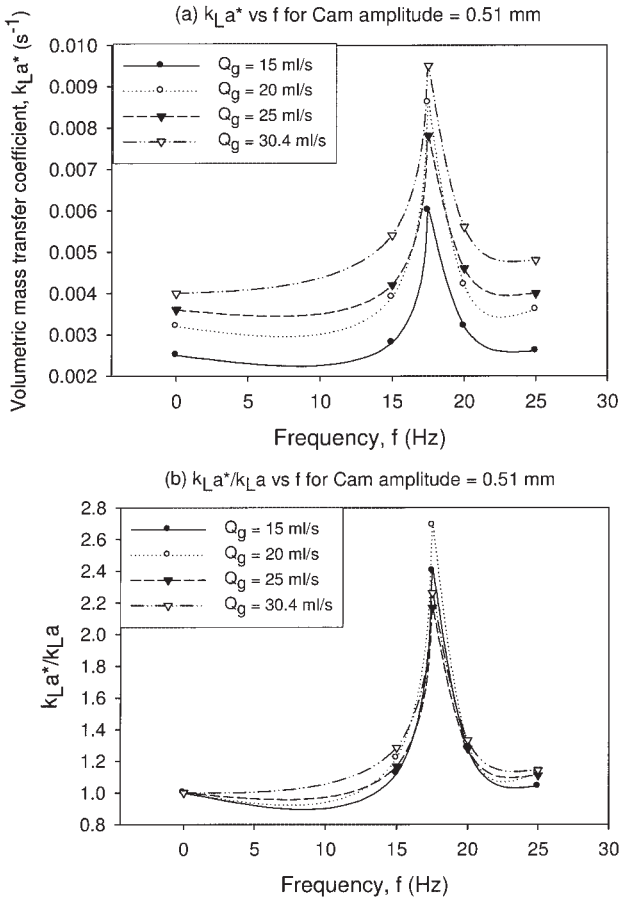

Figure 5. Volumetric mass-transfer coefficient as a function of frequency.

Cam amplitude = 0.51 mm, membrane thickness = 3.18 mm: (a) absolute k_La^*; (b) enhancement (k_La^*/k_La).

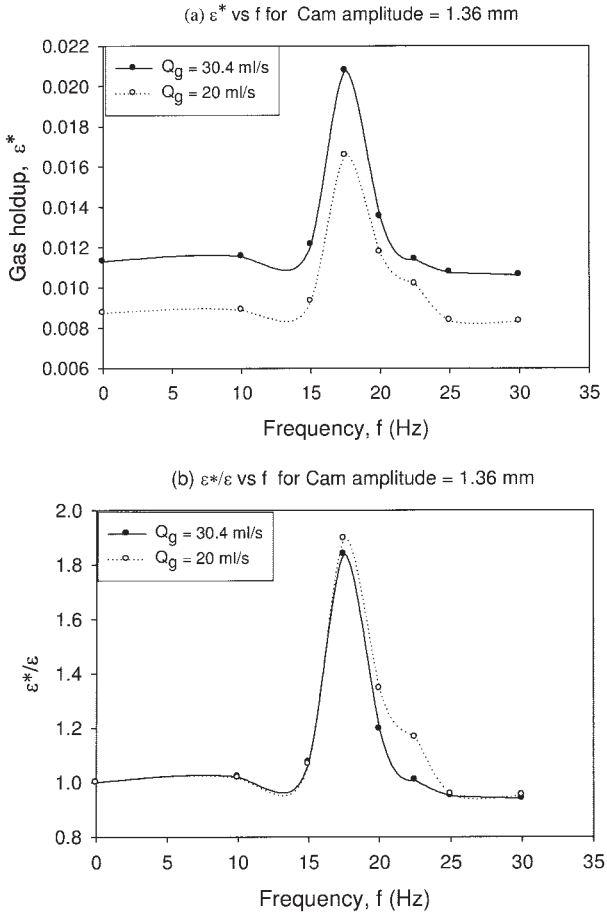

Figure 6. Gas hold-up as a function of frequency.

Cam amplitude = 1.36 mm, membrane thickness = 3.18 mm: (a) absolute ε^*; (b) enhancement $\varepsilon^*/\varepsilon$.

lowing recoalescence and thereby reducing voidage. During the run-up period, enhancement occurred mainly from increased "*a*," but also as a result of surface renewal by giving birth to new, smaller bubbles. This process continues as frequency and/or amplitude is increased until a critical, maximum stable bubble size is attained. Increases in frequency or amplitude beyond this serve only to cleanse the bubble surface and, at some point, bubble coalescence can arise, which serves to reduce voidage. The penetration of the boundary layer around the moving bubbles can be linked to the energy dissipation in the system, which increases with frequency and amplitude. It is also possible that small bubbles are retarded and move downward—attributed to the Bjerknes effect—and this may give rise to foaming and increased hold-up.

Applying the Benjamin–Ursell[15] stability theory to bubble breakage

We searched for an explanation for these somewhat curious results. It may be possible that the observed bubble breakup and enhanced mass transfer can be connected to the observed instability at the top interface.[16] When the free surface shows instability, as indicated by sloshing (Tables 1 and 2) and sloshing and/or foaming (Table 3), column performance is appreciably enhanced. The bubble breakup may be attributable to a "free-surface" instability on the almost horizontal interfaces of the large and very "flat" bottom interfaces on bubbles formed at the jetting injector, many of which took a spherical-cap shape. It seems plausible that large, spherical-cap bubbles can sustain interfacial oscillations in the same manner as the top interface. The flat bottom of the bubbles will behave just as any flat interface subjected to vibrations, except the flat surface is rising at a substantial rate.

Benjamin and Ursell[15] studied the unstable wave motion of the free surface (such as the air–water interface) of an inviscid liquid column subjected to vibrations at the base of the column. If a similar free surface instability is also created on the flat interfaces of large bubbles, then there is an engine to cause bubbles to break. Benjamin and Ursell[15] show, under the assumptions of small vibrational amplitude on an inviscid fluid, that the stability of the free surface is given by a series of Mathieu equations, which can sustain unstable behaviors at certain pulsing amplitudes and frequencies:

$$\frac{d^2a_m}{dT^2} + [p_m - 2q_m(\cos 2T)]a_m = 0 \tag{7}$$

where

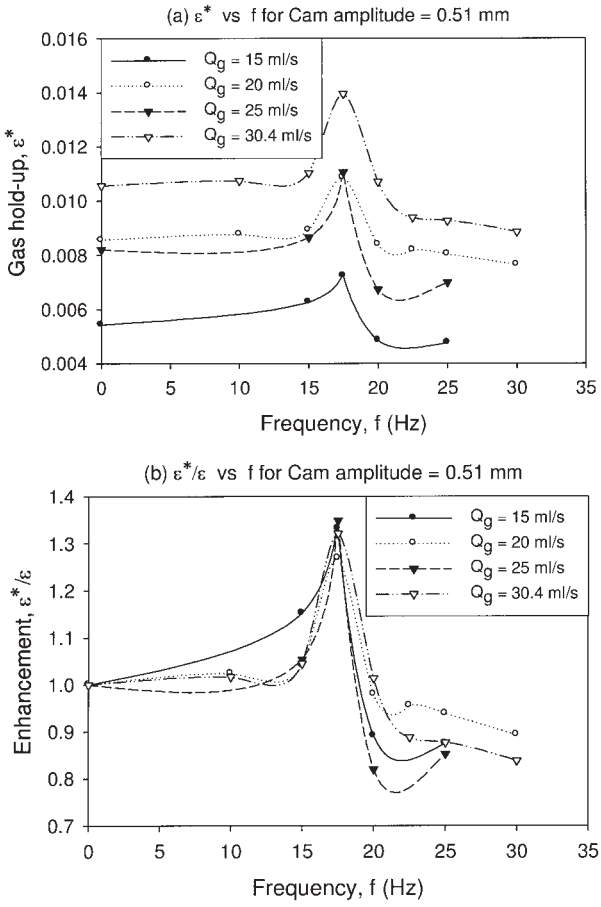

Figure 7. Gas hold-up as a function of frequency.

Cam amplitude = 0.51 mm, membrane thickness = 3.18 mm: (a) absolute ε^*; (b) enhancement $\varepsilon^*/\varepsilon$.

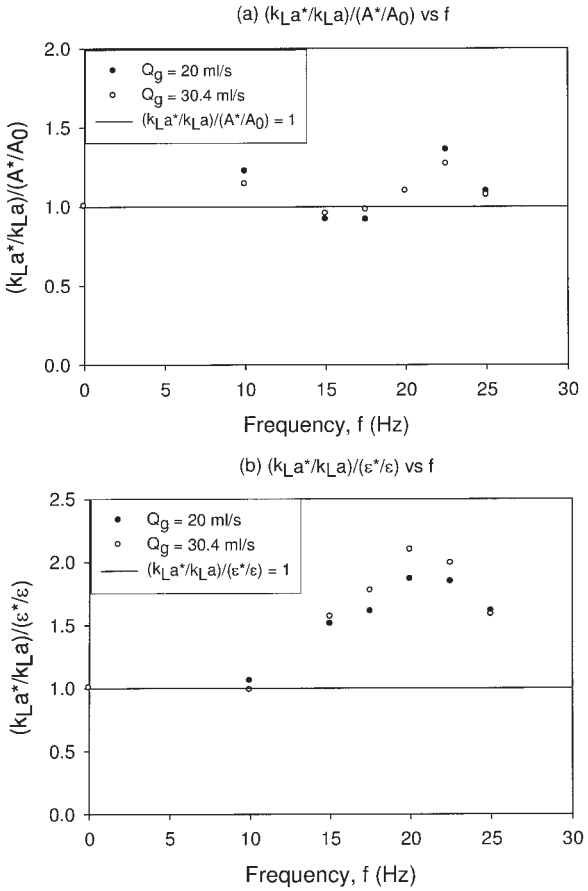

Figure 8. Comparison of flexible piston normalized mass transfer coefficient, gas hold-up, and water amplitude.

Cam amplitude = 1.36 mm, membrane thickness = 3.18 mm: (a) $(k_La^*/k_La)/(A^*/A_0)$ as a function of frequency; (b) $(k_La^*/k_La)/(\varepsilon^*/\varepsilon)$ as a function of frequency.

$$p_m = \left[\frac{4k_m \tanh(k_m h_w)}{\omega^2}\right]\left(g + \frac{k_m^2 \sigma}{\rho_l}\right) \tag{8}$$

$$q_m = 2k_m A \tanh(k_m h_w) \tag{9}$$

and a_m is the surface fluid amplitude, which is a function of time; k_m is the characteristic eigenvalue; ω is the forcing frequency (radians/s); A is the forcing amplitude (cm); h_w is the height of the water (cm), ρ_l is the water density = 1 g/cm^3; g is the acceleration arising from gravity = 981 cm/s^2; σ is the water surface tension = 72.5 dyn/cm; and T is $\omega t/2$, where t is the time in s.

For a vessel of cylindrical shape and radius R, k_m is an abbreviated form of $k_{P,m}$, where $J_P N(k_{P,m}R) = 0$. Here m denotes the mth zero of the derivative of the lth-order Bessel function, and $m = 1, 2, 3\cdots$ with $l = 0, 1, 2\cdots$. These eigenvalues are based on the condition of zero velocity at the vessel wall, where $r = R$.

The interesting results arising from the Benjamin–Ursell analysis led to a map of regions for stable and unstable behavior, using the dimensionless parameters p and q, which are proportional to the inverse square forcing frequency and forcing amplitude, respectively.

In Figure 10 (following Dodge[17]) we have plotted the solid piston data from Table 3 overlaid on the stability regions of Benjamin and Ursell.[15] Each frequency produces a constant p value and each fixed amplitude produces a constant q value. In Figure 10 we have used $(k_{l,m}R) = 11.706$, which is the fourth zero of the derivative of the first-order (thus, $l = 1$) Bessel function. There are countably infinite values of p_m and q_m for l, varying $l = 0, 1, 2\cdots$ and $m = 1, 2, 3\cdots$. The harmonics for $m = 4$, $l = 1$, were the lowest to yield p, q values in the unstable region for our particular column size (8.9 cm ID), so the calculations are based on the $k_{1,4}$ eigenvalue.

Our experiments showed surface instability closely followed that predicted by Benjamin and Ursell. There was good agreement between the regions of instability (free surface sloshing and/or foaming) predicted in Figure 10 and the experimental data of Table 3, except for the smallest tested amplitude of 0.46 mm. For example, at a constant amplitude of 1.23 mm, Figure 10 shows 0–15 Hz to be stable but 17.5–30 Hz to be unstable, and this was exactly as observed in the experiments shown in Table 3c. At the very small amplitude of 0.46 mm, Figure 10 shows that instability should occur at 20 Hz, but this was not experimentally observed. Such differences can be attributed to the effect of viscous damping, which are unaccounted for in this theory. Such damping, as estimated in Benjamin and Ursell's original work, shrinks the area of instability.

One could use the Benjamin–Ursell theory to predict the proper operating regions to gain large mass transfer and voidage enhancements. However, an even easier approach may be simply to vary the frequency, gradually increasing at a chosen cam setting, and wait for the surface to become unstable. There are several frequency ranges that produce instability on the free surface, although the first range (15–25 Hz in our experiments) is expected to have a strong performance enhancement in the column. In short, observation of the top surface gives fundamental information regarding instability several column diameters beneath the surface. We observed breakage to begin within approximately two column diameters of the injector, and continue close beneath the unstable top surface.

The question of instability imposed on the flat bottom surface or the top curved interface[18] of a rising spherical-cap bubble is an intriguing one. High-speed photographs of the fast rising spherical caps in a swarm of other bubbles was not possible in the present work. However, we propose that the Mathieu equation in the Benjamin–Ursell theory is the correct means to forecast behavior, provided the spherical-cap radius can be found, by calculation or observation. For example, if the spherical-cap bubble sustains a radius half the column diameter, then k_m is doubled and this at least doubles p_m and q_m, moving deeper into the unstable region.

Power dissipation under pulsing conditions

The power dissipation per unit mass of liquid has been widely used to correlate rates of mass transfer and mixing. For example, in an early and quite successful application, Baird and Rice[19] used the power input by the gas phase, undergoing a pressure drop equal to the hydrostatic head, to correlate the axial dispersion coefficient. Thus, the power provided by the gas injection, which is the product of velocity and force, is divided by liquid mass to yield

Table 3. Solid Piston Results[†]

(a) Piston amplitude = 2.46 mm					
At 0 Hz, $k_La = 0.004$ and $\varepsilon = 0.0067$					
F (Hz)	k_La^*	k_La^*/k_La	ε^*	$\varepsilon^*/\varepsilon$	Sloshing/foaming
10	0.006	1.5	0.0074	1.1	No
12.5	0.0085	2.125	0.0108	1.61	No
15	0.014	3.5	0.0153	2.28	Yes
17.5	0.025	6.25	0.0288	4.29	Yes
20	0.025	6.25	0.0288	4.29	Yes
25	0.025	6.25	0.0288	4.29	Yes
(b) Piston amplitude = 1.66 mm					
At 0 Hz, $k_La = 0.004$ and $\varepsilon = 0.0098$					
F (Hz)	k_La^*	k_La^*/k_La	ε^*	$\varepsilon^*/\varepsilon$	Sloshing/foaming
10	0.0065	1.625	0.0114	1.15	No
15	0.011	2.75	0.0139	1.40	Yes
17.5	0.018	4.5	0.0176	1.77	Yes
20	0.024	6	0.0193	1.94	Yes
22.5	0.0235	5.875	0.0207	2.08	Yes
25	0.022	5.5	0.0223	2.24	Yes
30	0.024	6	0.0313	3.15	Yes
(c) Piston amplitude = 1.23 mm					
At 0 Hz, $k_La = 0.004$ and $\varepsilon = 0.0067$					
F (Hz)	k_La^*	k_La^*/k_La	ε^*	$\varepsilon^*/\varepsilon$	Sloshing/foaming
10	0.0056	1.4	0.0090	1.35	No
15	0.0078	1.95	0.0105	1.58	No
17.5	0.011	2.75	0.0135	2.02	Yes
20	0.02	5	0.0229	3.43	Yes
22.5	0.019	4.75	0.0261	3.92	Yes
25	0.02	5	0.0278	4.17	Yes
30	0.02	5	0.0306	4.58	Yes
(d) Piston amplitude = 0.84 mm					
At 0 Hz, $k_La = 0.004$ and $\varepsilon = 0.0098$					
F (Hz)	k_La^*	k_La^*/k_La	ε^*	$\varepsilon^*/\varepsilon$	Sloshing/foaming
10	0.0052	1.3	0.0098	1.0	No
15	0.006	1.5	0.0110	1.1	No
17.5	0.008	2	0.0110	1.1	Yes
20	0.011	2.75	0.0121	1.21	Yes
25	0.0168	4.2	0.0233	2.33	Yes
30	0.017	4.25	0.0233	2.33	Yes
(e) Piston amplitude = 0.46 mm					
At 0 Hz, $k_La = 0.004$ and $\varepsilon = 0.0081$					
F (Hz)	k_La^*	k_La^*/k_La	ε^*	$\varepsilon^*/\varepsilon$	Sloshing/foaming
10	0.0048	1.2	0.0081	1.00	No
15	0.0052	1.3	0.0081	1.00	No
17.5	0.0052	1.3	0.0081	1.00	No
20	0.0054	1.35	0.0084	1.04	No
22.5	0.0065	1.625	0.0090	1.11	No
25	0.0092	2.3	0.0102	1.26	No
30	0.016	4	0.0207	2.56	Yes

[†] Membrane thickness = 3.18 mm; $Q_g = 30.4$ mL/s.

$$P_m = \frac{A_c U_{0g}[\rho_l(1-\varepsilon)h_0 g]}{A_c h_0 \rho_l (1-\varepsilon)} = U_{0g} g \tag{10}$$

A correlating function for power input per unit mass of liquid by the vibrating piston can be expressed in the dimensionally consistent framework as

$$P_m = \frac{A^2\omega^3}{2}$$

which is based on the time average of mass × acceleration (force) × the time average velocity. A physical model for P_m can be developed using the friction factor for circular tubes, as follows:

$$P_m = 2\,\frac{V(t)^3 \times f_f}{D_c}$$

where D_c is column diameter and f_f is the Fanning friction factor. For example, if the flow is laminar over most of the

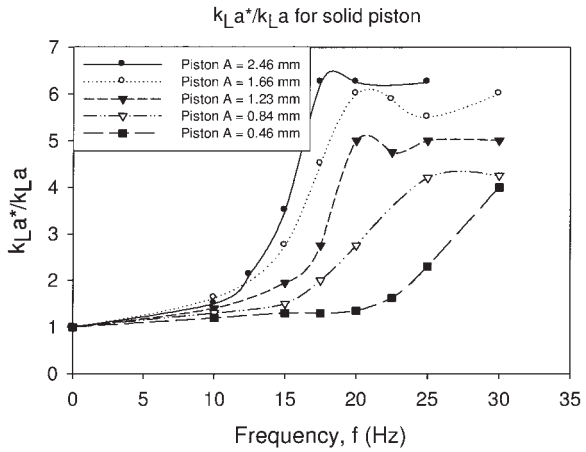

Figure 9. Enhancement (k_La^*/k_La) as a function of frequency for solid piston with different cam amplitudes.

Q_g = 30.4 mL/s, Membrane thickness = 3.18 mm.

cycle and $V(t) = A\omega \sin(\omega t)$, then the time-averaged power/mass is calculated using

$$P_m = \frac{16A^2\omega^2\nu}{D_c^2}$$

where ν is kinematic viscocity. For turbulent friction factors, finding the time average for a cycle is troublesome and not straightforward. For this reason, we elect to use the simple correlating function $A^2\omega^3/2$ to bring our data together, as illustrated in Figure 11, using the following equation for total power:

$$P_m^* = gU_{0g} + \frac{A^2\omega^3}{2} \tag{11}$$

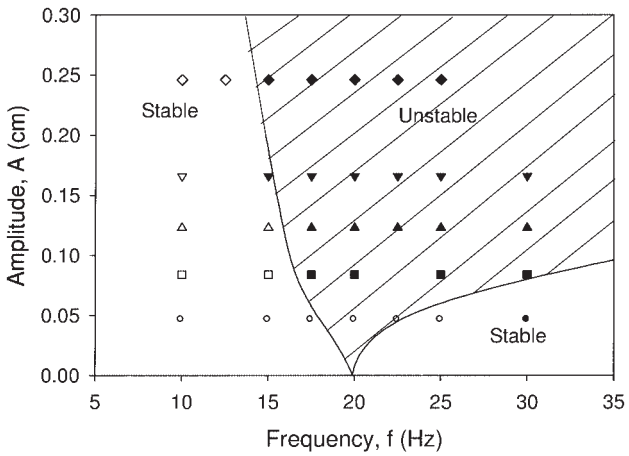

Figure 10. Mathieu's half-frequency stability chart for $\ell = 1$, $m = 4$ mode showing stable and unstable region.

Darkened data points represent unstable experimental responses, open point represent stable responses (see Table 3).

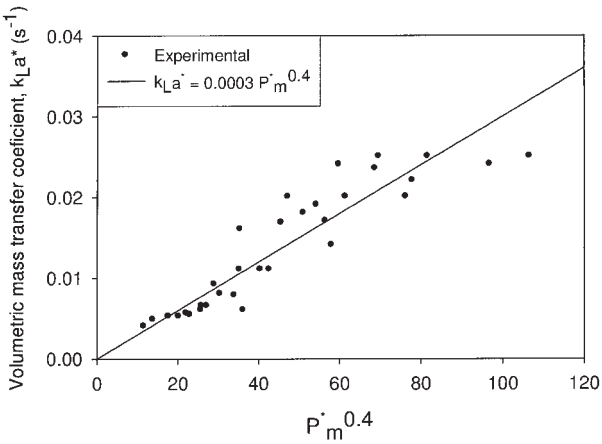

Figure 11. Volumetric mass-transfer coefficient vs. (power/mass)$^{0.4}$ for solid piston.

In these expressions, A denotes the liquid amplitude(half stroke length), which may also be a function of frequency for the flexible membrane piston, so in that case A is to be represented by A^* given in Tables 1 and 2 in Part I. In the calculation of mean velocity and acceleration, the root mean square values for the sinusoidal variations were taken over one period, which produced the square root of two in the denominator of each term.

It is difficult to correlate data that sustain maxima, but there have been attempts using power input to do just that.[20,21] Baird and Garstang[21] showed for pulsed columns with baffles that

$$k_La^* \propto (P_m^*)^{0.42}(U_{0g})^{0.5} \tag{12}$$

Similarly for columns with oscillating baffles Oliveira and Ni[22] found that

$$k_La^* \propto (P_m^*)^{0.4}(U_{0g})^{0.37} \tag{13}$$

Using these results, our solid piston data (Table 3) for volumetric mass transfer coefficient are plotted vs. (power/unit mass)$^{0.4}$ in Figure 11. There is good agreement between these data and the correlations in Eqs. 12 and 13.

Baird and Garstang[21] also found for their pulsed column that the voidage could be expressed as

$$\varepsilon^* \propto (P_m^*)^{0.42}(U_{0g})^{0.5} \tag{14}$$

Taking the ratio of Eq. 12 and Eq. 14,

$$k_La^* \propto \varepsilon^* \tag{15}$$

where Baird and Garstang[21] found $k_La^* = 0.75\varepsilon^*$. Plotting our solid piston volumetric mass transfer coefficient vs. voidage data in Figure 12 we found $k_La^* = 0.82\varepsilon^*$, which is in agreement with this early work. This interesting result implies that

$$k_L^* \propto d \tag{16}$$

given that spherical bubbles give

$$a = \frac{6}{d}\varepsilon^* \tag{17}$$

Equation 16 is contrary to Higbie's penetration theory, which suggests that k_L is proportional as

$$k_L \propto \sqrt{\frac{V_b}{d}} \tag{18}$$

Examination of Eq. 18 shows that k_L actually depends on both the rise velocity and bubble diameter. If the bubble rise velocity is slowing as a result of oscillations[3] or contamination of the interface causes immobility of the bubble film, then k_L^* becomes constant or slowly decreases, as observed by Harbaum and Houghton.[10]

In Figure 13 the flexible piston volumetric mass transfer coefficient vs. voidage data (Tables 1 and 2) is presented; here $k_La^* = 0.55\varepsilon^*$. Although this value differs from that of the solid piston, it is in agreement with the results of Krishna and Ellenberger,[1] who found $k_La^* = 0.5\varepsilon^*$.

We speculate that the dependency of volumetric mass transfer coefficient on voidage may depend on many factors, including the mechanism of vibration. Baird and Garstang[21] used a column with baffles, which may be more aligned with our solid piston. Krishna and Ellenberger[1] used an air dampener below their vibration source that may have acted similar to our flexible elastic membrane, which introduced viscoelasticity into the system. The difference between harsh and damped vibrations imposed on the system seems to be significant.

Conclusions

Active forcing to create bubble breakage produces distinctly different mechanisms under low gas flow rate (Part I) and high gas flow rate (Part II). Under appropriate forcing (pulsing) conditions and with low gas flow rate, bubble breakup involves both shearing in the injector and high velocity water slug impact of bubbles near the injector tip. At high gas flow rate, active forcing breaks bubbles in the column proper.

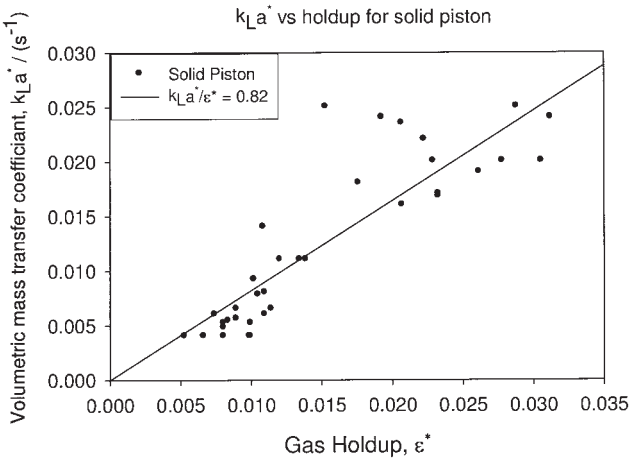

Figure 12. Volumetric mass transfer coefficient as a function of gas hold-up for solid piston.

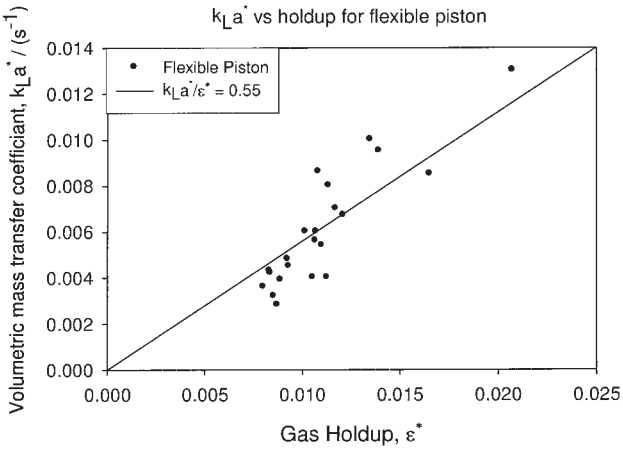

Figure 13. Volumetric mass transfer coefficient as a function of gas hold-up for flexible piston.

For high gas flow rates, the method of forcing—flexible piston or solid type piston—significantly affects bubble breakage dynamics. The flexible piston imparts the single resonant frequency of the membrane–water column system. The elasticity produces resonant amplitude much larger than expected from a simple solid piston motion. This causes high breakage rates in the frequency range surrounding that resonant frequency.

The solid piston behaves differently and, because the system does not sustain elastic resonance, a peak amplitude does not arise. Therefore some other explanation must be found for the breakage that occurred. This may be attributable to hydrodynamic instability at the flat bottoms of rising (large) spherical caps. The observed instability of the top column surface will extend at least several column diameters before it is damped. For the solid piston case, both hydrodynamic instability of the bottom interface of spherical caps, and breakup by the penetration of the unstable top interface into the rising bubbles contributes to breakup as a whole. For the flexible piston, in addition to the elastic resonance, the interface instability of the Benjamin–Ursell type will also be present. However, the elastic piston resonance seemed to produce less top surface instability, probably as a result of the inherent damping by the elastic membrane. It is interesting that the predicted bubble size according to Hinze's theory of breakage[23] is proportional to $1/(P_m)^{0.4}$, the same functional dependency we found for the solid piston. We conclude that the enhancements arise from two inextricably linked sources: power input and hydrodynamic instability.

Notation

a = gas–liquid interfacial area per unit volume of liquid, cm^2/cm^3
a_m = surface fluid amplitude, cm
A = water amplitude for solid piston (constant), mm
A_0 = water amplitude as frequency approaches zero, mm
A^* = water amplitude at particular forcing frequency for flexible piston, mm
A_c = column cross-sectional area, cm^2
C = oxygen concentration, $gmol/cm^3$
C^* = oxygen saturation concentration, $gmol/cm^3$
D = diffusion coefficient, cm^2/s

D_c = column diameter, cm
d = diameter of bubble, cm
F = force, dyn
f = frequency, Hz
f_f = Fanning friction factor, cm
g = acceleration arising from gravity, cm/s^2
H = distance between two taps, cm
h = mean depth of bubble, cm
h_0 = height of the water above injector tip under nonoscillating condition, cm
Δh = height difference between level of manometric fluid, cm
h_w = height of water in the column, cm
k_L = liquid-phase mass transfer coefficient, m/s
$k_L a$ = liquid-phase volumetric mass transfer coefficient, s^{-1}
$k_L a^*$= liquid-phase volumetric mass transfer coefficient vibrated case, s^{-1}
k_m = characteristic eigenvalue, dimensionless
L = mean depth of bubble below surface, cm
M = $\omega^4 A^2 \rho_l h/2gP_0$, dimensionless
m = denotes mth zero of $J_P N(k_{P,m}R)$
P_0 = pressure inside bubble, dyn/cm^2
P_m = power per unit mass without forcing, cm^2/s^3
P_m^* = power per unit mass with forcing, cm^2/s^3
p_m = as in Eq. 8, dimensionless
q_m = as in Eq. 9, dimensionless
Q_g = gas volumetric flow rate, cm^3/s
r_0 = bubble radius, cm
R = radius of column, cm
R_0 = orifice radius, cm
t = time, s
T = dimensionless time = $\omega t/2$, dimensionless
U_{0g} = superficial gas velocity, cm/s
V = velocity, cm/s
V_b = bubble rise velocity, cm/s
V_g = nozzle gas velocity, cm/s

Greek letters

ε = gas holdup, dimensionless
ε^* = gas holdup vibrated case, dimensionless
γ = specific heats ratio of gas (=1.4 for air), dimensionless
ν = kinematic viscosity, cm^2/s
ρ_g = gas density, g/cm^3
ρ_l = liquid density, g/cm^3
ρ_m = manometric fluid density, g/cm^3
σ = surface tension, dyn/cm
ω = frequency of oscillation, rad/s
ω_n = bubble system natural resonance frequency, rad/s

Literature Cited

1. Krishna R, Ellenberger J. Improving gas–liquid contacting in bubble columns by vibration excitement. *Int J Multiphase Flow*. 2002;28:1223-1234.
2. Ellenberger J, Krishna R. Improving mass transfer in gas–liquid dispersions by vibration excitement. *Chem Eng Sci.* 2002;57:4809-4815.
3. Ellenberger J, Krishna R. Shaken, not stirred, bubble column reactors: Enhancement of mass transfer by vibration excitement. *Chem Eng Sci.* 2003;58:705-710.
4. Ellenberger J, van Baten JM, Krishna R. Intensification of bubble columns by vibration excitement. *Catal Today.* 2003;79/80:181-188. [Also see website ct-cr4.chem.uva.nl/sonicsim/]
5. Bretsznajder S, Lesniewicz L, Pasiuk W. Influence of pulsation on the absorption of gases into liquids. *Bull Acad Polon Sci Ser Sci Chim Geol Geogr* 1959;7:591.
6. Harbaum KL, Houghton G. Effects of sonic vibrations on the rate of absorption of gases from bubble beds. *Chem Eng Sci.* 1960;13:90-92.
7. Baird MHI. Sonic resonance of bubble dispersions. *Chem Eng Sci.* 1963a;18:685-687.
8. Baird MHI. Resonant bubbles in a vertically vibrating liquid column. *Can J Chem Eng.* 1963b;4:52-55.
9. Minnaert M. On musical air-bubbles and the sounds of running water. *Philos Mag.* 1933;16:235.
10. Harbaum KL, Houghton G. Effects of sonic vibrations on the rate of absorption of carbon dioxide in gas bubble-beds. *J Appl Chem.* 1962;12:234-240.
11. Buchanan RH, Jameson G, Oedjoe D. Cyclic migration of bubbles in vertically vibrating liquid columns. *IEC Fundam.* 1962;1:82-86.
12. Wallis GB. *One-Dimensional Two-Phase Flow*. 1st Edition. New York, NY: McGraw-Hill; 1969.
13. Ma J. *Forced Bubble Columns.* MS Thesis. Baton Rouge, LA: Louisiana State University; 2003.
14. Burns LF. *The Effect of Reduced Surface Tension on Mass Transfer and Fluid Dynamics in Bubble Column Reactors* (*BCR*). MS Thesis. Baton Rouge, LA: Louisiana State University; 1995.
15. Benjamin TB, Ursell F. The stability of the plane free surface of a liquid in vertical periodic motion. *Proc R Soc Lond A Math Phys Sci.* 1954;225:505-515.
16. Connell KD. *Mass Transfer at an Oscillating Interface.* BS Thesis. Brisbane, Australia: University of Queensland; 1972.
17. Dodge FT. Vertical excitation of propellant tanks. In: Abramson HN, ed. *The Dynamic Behavior of Liquids in Moving Containers*. NASA-SP-0106. Washington, DC: NASA; 1966.
18. Kitscha J, Kocamustafaogullari G. Breakup criteria for fluid particles. *Int J Multiphase Flow.* 1989;15:573-588.
19. Baird MHI, Rice RG. Axial dispersion in large unbaffled columns. *Chem Eng J.* 1975;9:171-174.
20. Baird MHI, Garstang JH. Power consumption and gas hold-up in a pulsed column. *Chem Eng Sci.* 1967;22:1663-1673.
21. Baird MHI, Garstang JH. Gas absorption in a pulsed bubble column. *Chem Eng Sci.* 1972;27:823-833.
22. Oliveira MSN, Ni X. Gas hold-up and bubble diameters in a gassed oscillatory baffled column. *Chem Eng Sci.* 2001;56:6143-6148.
23. Geary NW, Rice RG. Bubble size prediction for rigid and flexible spargers. *AIChE J.* 1991;37:161-168.

Manuscript received Feb. 11, 2005, and revision received Aug. 26, 2005.